Synthesis, Characterization, and Rotational Dynamics of Crystalline Molecular Compasses with N-Heterocyclic Rotators

Braulio Rodriguez-Molina,[†,§] Ma. Eugenia Ochoa,[†] Norberto Farfán,*[,‡] Rosa Santillan,*[,†] and Miguel A. García-Garibay*[,§]

[†]Departamento de Química, Centro de Investigación y Estudios Avanzados del IPN, México D.F. 07360, México, [‡]Facultad de Química, Departamento de Química Orgánica, Universidad Nacional Autónoma de México, México D.F. 04510, México, and [§]Chemistry and Biochemistry Department, University of California, Los Angeles, California 90095

mgg@chem.ucla.edu; rsantill@cinvestav.mx; norberto.farfan@gmail.com
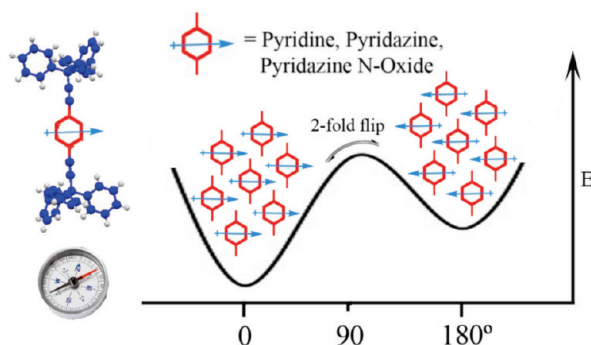
We describe in this paper the synthesis, crystallization, and solid-state NMR dynamics of molecules intended to emulate the structure and function of macroscopic compasses. The desired structures consist of polar pyridine (**2**) and pyridazine (**3**) groups as well as their corresponding *N*-oxides (**2O** and **3O**), each linked axially to two bulky triphenyl methyl groups by 1,4-triple bonds. The structures are such that the central polar heterocycles may rotate about the dialkyne axle while being sterically shielded by the two trityl groups. In addition to the synthesis of samples with natural isotopic abundance, we describe the preparation of **2**-d_2 and **3**-d_{30}, one labeled with deuteria in the pyridine rotator and the other fully deuterated in the two trityl groups in the stator. Crystal structures of **2** and **3** revealed packing motifs analogous to those previously reported for samples prepared with substituted phenylene rotators. While solid-state NMR measurements by ^{13}C CPMAS NMR revealed insufficient chemical shift dispersion for a dynamic characterization of the rotation of compounds **2** and **3** (including **3**-d_{30}), the use of quadrupolar echo ^{2}H NMR methods with **2**-d_2 revealed a rotational site exchange with a barrier of ca. 8.5 kcal/mol (35.5 kJ mol^{-1}) for the pyridine group in **2**.

Introduction

The synthesis of molecules that emulate the structure and motion of macroscopic devices has been a subject of great interest over the last few years.[1] While most studies are carried out with molecules in solution, recent efforts have addressed the potential function of molecules bound to surfaces[2,3] and in the

(1) (a) Kay, E. R.; Leigh, D. A.; Zerbetto, F. *Angew. Chem., Int. Ed.* **2007**, *46*, 72. (b) Marsella, M. J.; Rahbarnia, S.; Wilmont, N. *Org. Biomol. Chem.* **2007**, *5*, 391. (c) Skopek, K.; Hershberger, M.C.; Gladysz, J.A. *Coord. Chem. Rev.* **2007**, *251*, 1723. (d) Shirai, Y.; Morin, J.-F.; Sasaki, T.; Guerrero, J. M.; Tour, J. M. *Chem. Soc. Rev.* **2006**, *35*, 1043. (e) Kottas, G. S.; Clarke, L. I.; Horinek, D.; Michl *Chem. Rev.* **2005**, *105*, 1281. (f) Balzani, V.; Margherita, V.; Credi, A. *Molecular Devices and Machines*; Wiley-VCH: Weinheim, 2003. (g) Feringa, B. L.; Koumura, N.; Delden, R. A.; TerWiel, M. K. *Appl. Phys. A* **2002**, *75*, 301. (h) Sestelo, J. P.; Kelly, T. R. *Appl. Phys. A* **2002**, *75*, 337. (i) Balzani, V.; Credi, A.; Raymo, F.; Stoddart, F. *Angew. Chem., Int. Ed.* **2000**, *39*, 3349.

(2) (a) Horinek, D.; Michl, J. *Proc. Nat. Acad. Sci. U.S.A.* **2005**, *102*, 14175. (b) Vacek, J.; Michl, J. *Adv. Funct. Mater.* **2007**, *17*, 730. (c) Zheng, X.; Mulcahy, M. E.; Horinek, D.; Galeotti, F.; Magnera, T.; Michl, J. *J. Am. Chem. Soc.* **2004**, *126*, 4540. (d) Balzani, V.; Credi, A.; Venturi, M. *ChemPhysChem* **2008**, *9*, 202.

(3) (a) Shirai, Y.; Morin, J. F.; Sasaki, T.; Guerrero, J. M.; Tour, J. M. *Chem. Soc. Rev.* **2006**, *35*, 1043. (b) Shirai, Y.; Osgood, A. J.; Zhao, Y.; Saudan, L.; Yang, H.; Yu-Hung, C.; Alemany, L. B.; Sasaki, T.; Morin, J. F.; Guerrero, J. M.; Kelly, K. F.; Tour, J. M. *J. Am. Chem. Soc.* **2006**, *128*, 4854. (c) Sasaki, T.; Osgood, A. J.; Alemany, L. B.; Kelly, K. F.; Tour, J. M. *Org. Lett.* **2008**, *10*, 229.

(4) (a) Karlen, S. D.; Garcia-Garibay, M. A. *Top. Curr. Chem.* **2006**, *262*, 179. (b) Khuong, T.A.; Nuñez, J.E.; Godinez, C.E.; García-Garibay, M.A. *Acc. Chem. Res.* **2006**, *39*, 413. (c) Garcia-Garibay, M. A. *Proc. Nat. Acad. Sci. U.S.A.* **2005**, *102*, 10771.
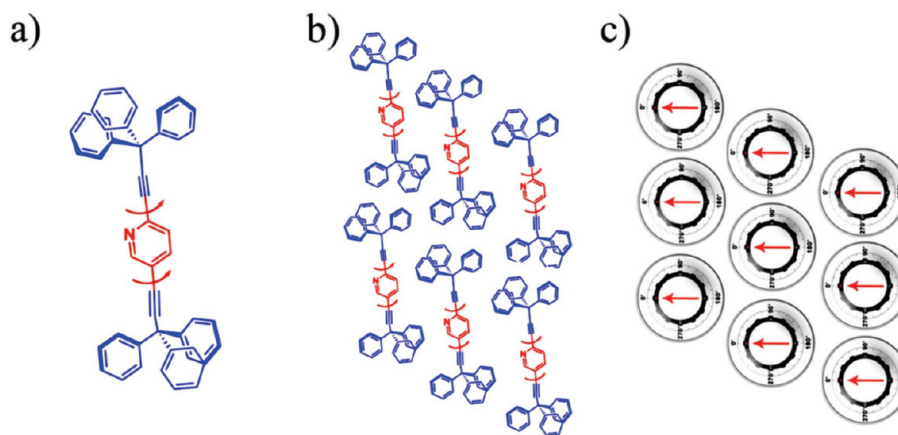
FIGURE 1. (a) Line formula of a molecular compass with a polar pyridine rotator as a representative of other nitrogen heteroaromatics and (b) representation of a crystalline array of molecular compasses and the suggested analogy to (c) an array of macroscopic compasses.

solid-state.[4−6] In that context, our group has been interested in exploring the properties of crystals made up of molecular rotors[7] intended to emulate the structures and function of macroscopic compasses and gyroscopes (Figure 1).[4,8]

With structures consisting of substituted phenylene rotators linked by triple bonds to bulky triarylmethanes, we have described the formation of crystals that support an internal rotation consisting of a site exchange between energy minima related by angular displacements of 180°.[4,9] With structural elements that are relatively static linked to others that are highly mobile, we suggested the term *amphidynamic* crystals to highlight the dynamic properties of these materials.[4] Using metal organic frameworks[10] and molecular crystals with nonpolar rotators, we have shown that variations in the size and topology of the stator[11] and on the size and rotational symmetry order of the stator[12] have a deep influence on their internal dynamics in the solid state. However, it has

been suggested that optimal structures of dipolar arrays formed by the introduction of polar substituents on the rotator will provide opportunities for a new class of materials based on physical properties that change with the orientation of reorienting dipoles as a function of internal and external fields.[4,5a,13,14] Among the structural features expected to influence the dynamic and electric behavior of such materials are their barriers to rotation, the magnitude of their dipole moments, as well as their distances, relative orientations, and lattice symmetries.[13] Other things being equal, smaller rotators are expected to have fewer steric interactions and lower rotational barriers and greater dipoles are expected to have stronger interactions with neighboring dipoles and external fields.

We previously reported a set of molecular compasses with monosubstituted phenylene rotators having fluoro (**1b**), amino (**1c**), cyano (**1d**), and nitro (**1e**) substituents (Scheme 1).[9,15,16] Compounds **1b**−**e** have calculated dipole moments between 1.49 and 4.74 D and molecular volumes that increase modestly by ca. 0.96 to 4.1% as compared to that of **1a**.[17] In spite of their reduced molecular symmetries, these compounds were shown to have molecular and packing structures analogous to those of the parent hydrocarbon **1a**. Crystals were obtained in a solvent-free environment grown from CH_2Cl_2 and in a solvent chlathrate in the presence of benzene, both in the triclinic space group P-$\bar{1}$.[9,15] A third packing structure in the monoclic space group $P2_1/c$ was obtained with compound **1d** from a mixture of hexane and EtOAc.[15] The two types of triclinic crystals were characterized by having only one molecule per unit cell with the polar

(5) (a) Akutagawa, T.; Koshinaka, H.; Sato, D.; Takeda, S.; Noro, S.-I.; Takahashi, H.; Kumai, R.; Tokura, Y.; Nakamura, T. *Nature Mater.* **2009**, *8*, 342. (b) Trolliet, C.; Poulet, G.; Tuel, A.; Wuest, J. D.; Sautet, P. *J. Am. Chem. Soc.* **2007**, *129*, 3621. (c) Horike, S.; Matsuda, R.; Tanaka, D.; Matsubara, S.; Mizuno, M.; Endo, K.; Kitagawa, S. *Angew. Chem., Int. Ed.* **2006**, *43*, 7226. (d) Sato, D.; Akutagawa, T.; Takeda, S.; Noro, S.; Nakamura, T. *Inorg. Chem.* **2007**, *46*, 363. (e) Sato, N.; Nishikiori, S.I. *Dalton Trans.* **2007**, 1115. (f) Zhou, W.; Yildirim, T. *Phys. Rev. B* **2006**, *74*, 180301.

(6) Sokolov, A. N.; Swenson, D. C.; MacGillivray, L. R. *Proc. Nat. Acad. Sci. U.S.A.* **2008**, *105*, 1794.

(7) Adopting the nomenclature suggested in ref 1e, we will use the term molecular rotor to refer to the entire molecule, in this case as a synonym of the term "molecular compass". A molecular rotor itself is an assembly that consists of a stator and rotator that are linked by an axle.

(8) For an overview of molecular structures that emulate certain aspects of macroscopic gyroscopes, see: Skopek, K.; Hershberger, M. C.; Gladysz, J. A. *Coord. Chem. Rev.* **2007**, *251*, 1723.

(9) (a) Dominguez, Z.; Dang, H.; Strouse, M. J.; Garcia-Garibay, M. A. *J. Am. Chem. Soc.* **2002**, *124*, 2398. (b) Godinez, C. E.; Zepeda, G.; Garcia-Garibay, M. A. *J. Am. Chem. Soc.* **2002**, *124*, 4701.

(10) Gould, S. L.; Tranchemontagne, D.; Yaghi, O. M.; Garcia-Garibay, M. A. *J. Am. Chem. Soc.* **2008**, *130*, 3246.

(11) (a) Khuong, T.A.V.; Zepeda, G.; Ruiz, R.; Kahn, S. I.; Garcia-Garibay, M.A. *Cryst. Growth Des.* **2004**, *4*, 15. (b) Godinez, C. E.; Zepeda, G.; Mortko, C. J.; Dang, H.; Garcia-Garibay, M. A. *J. Org. Chem.* **2004**, *69*, 1652. (c) Karlen, S. D.; Godinez, C. E.; Garcia-Garibay, M. A. *Org. Lett.* **2006**, *8* 3417. (d) Karlen, S. D.; Khan, S. I.; Garcia-Garibay, M. A. *Mol. Cryst. Liq. Cryst.* **2006**, *456*, 221. (e) Khuong, T.-A. V.; Dang, H.; Jarowski, P. D.; Emily, F.; Maverick; Garcia-Garibay, M. A. *J. Am. Chem. Soc.* **2007**, *129*, 839. (f) Jarowski, P.D.; Houk, K. N.; Garcia-Garibay, M.A. *J. Am. Chem. Soc.* **2007**, *129*, 3110. (g) Nuñez, J. E.; Natarajan, A.; Khan, S. I.; Garcia-Garibay, M. A. *Org. Lett.* **2007**, *9*, 3559. (h) Gould, S. L.; Rodriguez, R. B.; Garcia-Garibay, M A. *Tetrahedron* **2008**, *64*, 8336.

(12) Karlen, S. D.; Ortiz, R; Chapman, O. L.; Garcia-Garibay, M. A. *J. Am. Chem. Soc.* **2005**, *127*, 6554.

(13) (a) Michl, J.; Sykes, C.H. *ACS Nano* **2009**, *3*, 1042. (b) Horinek, D.; Michl, J. *J. Am. Chem. Soc.* **2003**, *125*, 11900. (c) de Jonge, J.J.; Ratner, M.A.; de Leeuw, S.W. *J. Phys. Chem. C* **2007**, *111*, 3770.
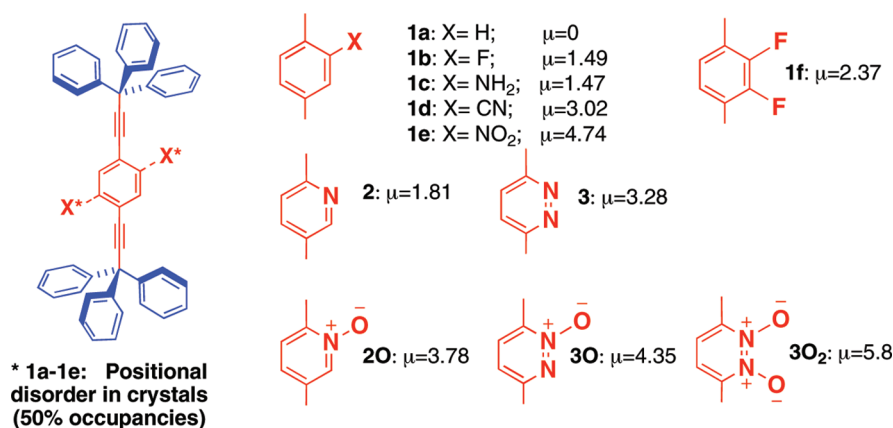
(14) (a) Salech, B. E. A; Teich, M. C *Fundamentals of Photonics*; Wiley-Interscience: New York, 1991. (b) Weber, M. J. *Handbook of Optical Materials*; CRC Press: Boca Raton, 2002. (c) Setian, L. *Applications in Electrooptics*; Prentice Hall: New York, 2001.

(15) Dominguez, Z.; Khuong, T. A. V.; Sanrame, C. N.; Dang, H.; Nuñez, J. E.; Garcia-Garibay, M. A. *J. Am. Chem. Soc.* **2003**, *125*, 8827.

(16) Compounds with 2,3-diamino and 2-nitro-5-amino substituents were also reported in ref 15.

(17) The volume and dipole moment values calculated in this study for structures minimized with the AM1 method using the program Spartan are as follows: **1a**, 606 $\mathring{A}^3$ and 0 D; **1b**, 611.8 $\mathring{A}^3$ and 1.49 D; **1c**, 618.4 $\mathring{A}^3$ and 1.47 D; **1d**, 625.6 $\mathring{A}^3$ and 3.02 D; **1e**, 630.9 $\mathring{A}^3$ and 4.74 D; **1f**, 617.2 $\mathring{A}^3$ and 2.37 D; **2**, 602.8 $\mathring{A}^3$ and 1.81 D; **3**, 599.2 $\mathring{A}^3$ and 3.28 D; **2O**, 611.5 $\mathring{A}^3$ and 3.78 D; **3O**, 607.8 $\mathring{A}^3$ and 4.35 D.

SCHEME 1

1a: X= H; μ=0
1b: X= F; μ=1.49
1c: X= NH$_2$; μ=1.47
1d: X= CN; μ=3.02
1e: X= NO$_2$; μ=4.74

1f: μ=2.37

2: μ=1.81

3: μ=3.28

2O: μ=3.78

3O: μ=4.35

3O2: μ=5.8

* **1a-1e:** Positional
disorder in crystals
(50% occupancies)

group positionally disordered with 50% occupancies in sites related by a crystallographic center of inversion, which coincides with a molecular center of inversion only in the case of structure **1a** (Scheme 1). With the bulky trityl groups determining the packing structures, an increase in the size of the polar substituent resulted in higher rotational barriers and rotational rates that are too small to measure for substituents with sizes larger than that of fluorine. Notably, the activation energies for rotation determined with a combination of variable-temperature (VT) ^{13}C CPMAS NMR and quadrupolar echo ^{2}H NMR line shape analysis showed that the barrier in the solvent-free samples increases by ca. 1 kcal/mol (4.184 kJ mol^{-1}), from 12.8[9,15] to 13.7[18] to 14.8[19] kcal/mol (53.5, 57.3, and 61.9 kJ mol^{-1}, respectively), as the rotator varies from phenylene (**1a**) to 2-fluorophenylene (**1b**) to 2,3-difluorophenylene (**1f**).

In this paper, we report our analysis of nitrogen heteroaromatics **2**, **3**, **2O**, **3O**, and **3O2** as potential polar molecular rotators. Our motivation comes from the fact that pyridine and pyridazine rotators in **2** and **3** have greater dipole moments (1.81 and 3.28 D)[17] than those of fluorobenzene and 2,3-difluorobenzene in **1a** and **1f** (1.49 and 2.37 D). An additional incentive comes from the fact that pyridine and pyridazine are smaller than phenylene by ca. 0.5% and 1.1%, respectively,[17] and might display faster rotational motion if they adopt isomorphous packing structures. Furthermore, the nitrogen heterocycles in **2** and **3** may be transformed into the corresponding N-oxides **2O** and **3O**, and perhaps the N,N-dioxides **3O2**, which have greater dipole moments with sizes that are very similar to those of the mono- and difluorinated **1b** and **1f**.[17] In the sections that follow, we describe the synthesis and characterization of the two heterocyclic rotors. While the pyridine and pyridazine oxides could be prepared by oxidation with m-CPBA, only **3O** was reasonably persistent. The pyridazine N,N-dioxide **3O2** could not be obtained under similar reaction conditions. We report the crystal structures of **2**, **3**, and **3O** and a detailed solid-state ^{13}C CPMAS NMR characterization of polycrystalline samples of **2** and **3**. Having discovered that compound **3** lacks the chemical shift resolution needed to detect

the pyridazine signals for dynamic studies using variable-temperature ^{13}C NMR, we prepared a sample of **3**-d_{30} with a fully deuterated trityl stator in order to remove all the interfering ^{13}C signals in a CPMAS experiment. Unfortunately, ^{13}C CPMAS NMR measurements with **3**-d_{30} showed a broad pyridazine carbon signal with insufficient resolution or chemical shift dispersion to observe splitting indicative of site exchange. Similarly, while samples of polycrystalline **2** showed ^{13}C CPMAS NMR spectra with line shape changes consistent with an exchange process, insufficient chemical shift dispersion was not conducive to useful rate determinations by line-shape analysis. Fortunately, samples of 3,4-d_2-2,5-dibromopyridine became available by base-catalyzed ^{2}H exchange and were used to prepare pyridine-labeled **2**-d_2, which revealed a barrier of ca. 8.5 kcal/mol (35.5 kJ mol^{-1}) by analysis of their variable-temperature (VT) quadrupolar echo ^{2}H NMR spectra. Remarkably, this barrier is about 4−6 kcal/mol (16.7−25.1 kJ mol^{-1}) lower than those of the parent hydrocarbon **1a** and its fluorinated derivatives **1b** and **1f**. Unfortunately, we were not successful in our attempts to prepare samples of deuterium-labeled pyridazine for analogous studies with compound **3**.

Results and Discussion

Synthesis of Molecular Rotors. Compounds **2** and **3** were synthesized by Pd(0)-catalyzed cross coupling between the appropriate 3,3,3-triphenyl-1-propyne **4** and the corresponding disubstituted heteroaromatic rotator in a fashion analogous to that in a previously described methodology (Scheme 2). Samples of 3,3,3-triphenyl-1-propyne **4** were obtained in 95% yield by reaction of trityl chloride with 4 equiv of ethynylmagnesium bromide in dry benzene under reflux. Samples of 3,3,3-triphenyl-1-propyne-d_{15} (compound **4**-d_{15}, Scheme 3) were obtained by Friedel−Crafts reaction of benzene-d_6 with CCl$_4$ and AlCl$_3$ affording chlorotris-(phenyl-d_5)methane as previously described.[20] The halogenated product was treated under reflux with an excess of ethynylmagnesium bromide in benzene to give the desired product. Samples of **2O** and **3O** were obtained by m-chloroperbenzoic acid (m-CPBA) oxidation of **2** and **3**.
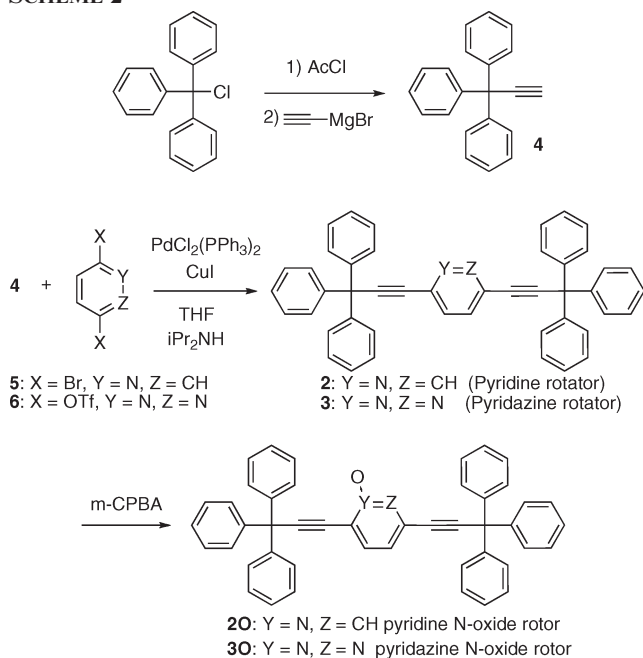
The pyridine-containing molecular rotor **2** was prepared in 80% yield through Sonogashira cross coupling between

(18) Santillan, R.; Karlen, S. D.; Dang, H.; Garcia-Garibay, M. A. *J. Mex. Chem. Soc.* **2008**, *52*, 125.
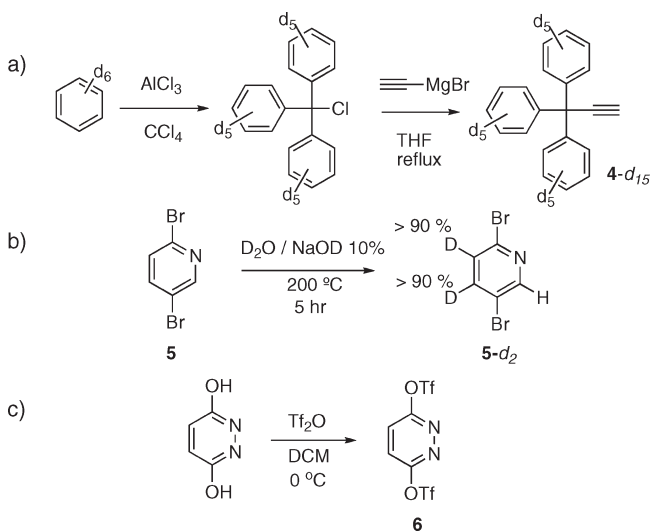
(19) Horansky, R. D; Clarke, L; Winston, E; Price, J. C; Karlen, S. D; Jarowski, P. D; Santillan, R; Garcia-Garibay, M. A. *Phys. Rev. B* **2006**, *74*, 054306.

(20) Karlen, S. D.; Garcia-Garibay, M. A. *Chem. Commun.* **2005**, 189.

SCHEME 2

SCHEME 3

commercially available 2,5-dibromopyridine **5** (Scheme 2) and trityl acetylene **4**. All of the Pd(0)-coupling reactions were carried out under Sonogashira conditions by reflux with Pd$_2$Cl$_2$(PPh$_3$)$_2$, CuI, and *i*-Pr$_2$NH under N$_2$ or Ar atmosphere in freshly distilled THF.[21] Coupling products were often obtained with a small amount of hexaphenylbutadiyne **8** (Scheme 4) as a side product,[22] and purifications were carried out by column chromatography with a ternary mixture of hexanes, CH$_2$Cl$_2$, and EtOAc as the eluent using silica gel (for compounds **2**, **2**-*d$_2$*, **3**, and **3**-*d$_{30}$*) or alumina

(for *N*-oxides **2O** and **3O**). Samples of 2,5-dibromopyridine-*d$_2$* **5**-*d$_2$* for the synthesis of molecular compass **2**-*d$_2$* were prepared by deuterium exchange of **5** with NaOD in D$_2$O (Scheme 3b). The reaction proceeded in a reasonable yield of 65% with selective (> 90%) deuterium exchange at positions C-3 and C-4 of the heteroaromatic ring, as determined by ^{1}H and ^{13}C NMR. Samples of 2,5-dibromopyridine and its deuterated analogue **5** and **5**-*d$_2$* afforded products **7** and **7**-*d$_2$* by C−C coupling at the carbon *ortho* to the nitrogen. This observation is in agreement with previous results, which have shown that analogous reactions can be accelerated by the electron withdrawing effects of the heteroatom.[23] Molecular compasses **2** and **2**-*d$_2$* were obtained in similar yields in two steps by separating and purifying the mono-coupling product followed by a second coupling reaction or by adding an excess of the alkyne and increasing the reaction time.

The pyridazine-containing structure **3** was obtained in 75% yield from 3,6-pyridazinediol ditriflate **6** (Scheme 3c). The latter was readily accessible from a stirred solution of commercial 3,6-pyridazinediol and triflic anhydride in dichloromethane at 0 °C. Compound **3**-*d$_{30}$* was synthesized by reaction of 2.5 equiv of 3,3,3-triphenyl-1-propyne-*d$_{15}$* (**4**-*d$_{15}$*)[24] with 3,6-pyridazinediol ditriflate **6**. Pure samples of molecular compasses **2** and **3** were treated with *m*-chloroperbenzoic acid to afford pyridine *N*-oxide rotor **2O**, which rapidly decomposes in solution, and the more stable pyridazine *N*-oxide rotor **3O**, respectively.[25] Attempts to prepare pyridazine *N*,*N*-dioxide **3O2** from samples of purified **3O** led to complex product mixtures, and the synthesis of this compound was not pursued further.

Spectroscopic Characterization. While spectroscopic analysis by ^{1}H and ^{13}C NMR of molecular compasses with pyridine (**2**, **2**-*d$_2$*), pyridazine (**3**, **3**-*d$_{30}$*), and pyridazine *N*-oxide (**3O**) gave results that conformed to our expectations, we found that samples of pyridine *N*-oxide **2O** decompose very rapidly in solution. High-resolution ESI-TOF mass spectra gave abundant parent ions for all compounds, and analysis by FT-IR showed relatively weak stretching bands for the disubstitued triple bonds. Single crystals suitable for X-ray diffraction analysis were obtained for the pyridine rotor **2** and the pyridazine rotor **3**. The single crystal of the pyridazine *N*-oxide rotor **3O** was of lower quality, but a reliable structure could be obtained.

A summary of the ^{1}H and ^{13}C NMR data is included in Tables 1 and 2. The atom numbering used in these tables is different from that used in the crystal structures to reflect their different symmetries and magnetically different nuclei. While the presence of a nitrogen atom in compound **2** makes the two halves of the molecule different and carbons C1−C19 in Table 1 magnetically nonequivalent, the crystal structure shows the two sides to be crystallographically equivalent by an average inversion center that results from the disorder of the nitrogen atom with a 50% occupancy over the two inversion related sites (vide infra). Conversely, molecular rotor **3** has an average mirror plane with magnetically equivalent carbons C1−C9 in solution, but the two halves of the molecule are crystallographic nonequivalent in

(21) (a) Chinchilla, R.; Najera, C. *Chem. Rev.* **2007**, *107*, 874 and references cited therein. (b) Sonogashira, K.; Tohda, Y.; Hagihara, N. *Tetrahedron Lett.* **1975**, *50*, 4467.

(22) (a) Li, D. F.; Yin, K.; Li, J.; Jia, X. S. *Tetrahedron Lett.* **2008**, *49*, 5918. (b) Batsanov, A. S.; Collings, J. C.; Fairlamb, I. J. S.; Holland, J. P.; Howard, J. A. K.; Lin, Z. Y.; Marder, T. B.; Parsons, A. C.; Ward, R. M.; Zhu, J. *J. Org. Chem.* **2005**, *70*, 703.

(23) (a) Tilley, J. W.; Zawoiski, S. *J. Org. Chem.* **1988**, *53*, 386. (b) Singh, R.; Just, G. *J. Org. Chem.* **1989**, *54*, 4453.

(24) Karlen, S.D.; Garcia-Garibay, M.A. *Chem. Commun.* **2005**, 189.

(25) Caron, S.; Do, N. M.; Sieser, J. E. *Tetrahedron Lett.* **2000**, *41*, 2299.

SCHEME 4
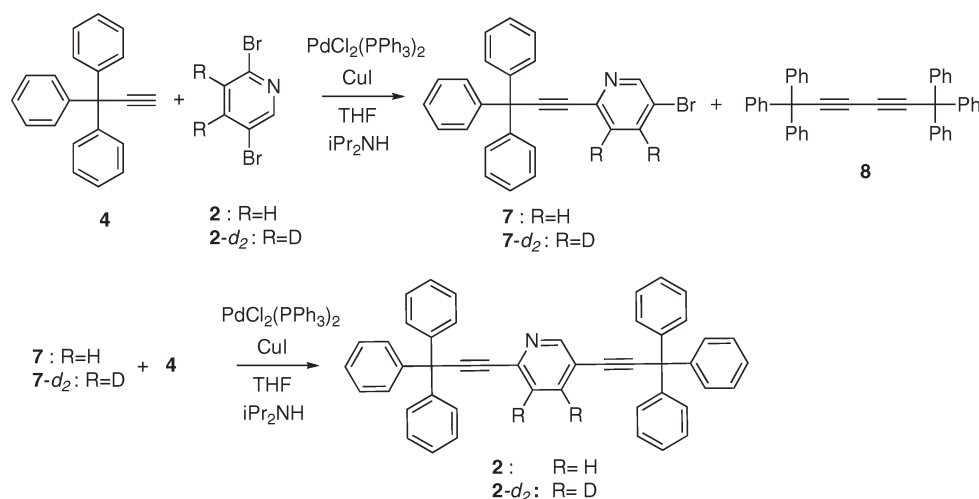
TABLE 1.   ^{1}H NMR Signals from Central Rotators of Molecular Compasses **2**, **3**, and **3O** in CDCl$_3$

[1]H Signal	**2** δ (J$_{HH}$, Hz)[a]	**2**-d_2 δ (J$_{HH}$)[b]	**3**[c] δ	**3**-d_{30}[a] δ	**3O** δ (J$_{HH}$, Hz)[c]
H1	7.72 d (8.2)	--	7.51	7.50	7.65 d (8.2)
H10	7.39 dd (8.2, 2.0)	--	--	--	7.08 d (8.2)
H19	8.70 d (2.0)	8.70 s	--	--	--

[a]Data determined with NMR spectrometer operating at 500 MHz. [b]Data determined with NMR spectrometer operating at 300 MHz. [c]Data determined with NMR spectrometer operating at 400 MHz.

the solid state (vide infra). The atom numbering for molecular compass **3O** was kept in agreement with that of **3** in order to highlight their differences in chemical shifts.

The ^{1}H NMR signals from the central rings in compounds **2**, **3**, and their deuterated isotopologs, **2**-d_2, and **3**-d_{30} are summarized in Table 1 along with those of **3O**. In the case of pyridine rotator **2**, the signal of H1 appears at δ 7.72 ppm as a doublet due to the ^3J = 8.2 Hz coupling with H10, which in turn appears at δ 7.39 ppm as a doublet of doublets with ^3J = 8.2 Hz and ^4J = 2.0 Hz due to further coupling with H19. As expected from its neighboring relation to the nitrogen atom, the latter is the most deshielded signal with a chemical shift δ 8.70 ppm. After deuterium exchange in C1 and C10 of the pyridine ring, the chemical shift of the signal at H19 remains unaltered in rotor **2**-d_2, but the scalar coupling disappears from the spectrum. Weak residual peaks in ^{1}H NMR (< 10 % intensity) from nondeuterated isotopologs were observable.

In the case of the pyridazine-containing compounds **3** and **3**-d_{30}, only the singlet corresponding to H1 was observed at δ 7.51 ppm with the hydrogens from the trityl groups appearing as multiplets from δ 7.42 to δ 7.26 ppm in **3**. Small residual signals were observed for the stators of **3**-d_{30}, which had been prepared from isotopically enriched benzene-d_6 (99.6 %). While samples of *N*-oxide **3O** slowly decomposed in solution, signals at δ 7.65 and δ 7.08 ppm with a scalar coupling of

^3J = 8.2 Hz could be assigned to H1 and H10 of the central rotator, respectively, by comparison with reports describing the NMR shifts of unsubstituted pyridazine *N*-oxides.[26]

Selected ^{13}C NMR shifts obtained under broadband ^{1}H decoupling in solution are presented in Table 2. The spectra corresponding to molecular compasses **2** and **3O** showed readily distinguishable signals for the two nonequivalent halves of the molecules and all of the chemically distinct carbons of the central rotators. The solution spectrum of **3** was significantly simpler with only nine signals due to the time-average mirror symmetry of the structure. The spectra from the deuterated samples **2**-d_2 and **3**-d_{30} showed only very small residual signals for the deuterated carbons, as expected from the lack of nuclear Overhauser effect and by the signal splitting that occurs as a result of scalar coupling with the ^2H nuclei. Listed in Table 2 are all the signals from the central diethynyl heteroaromatic moiety, C1−C5 and C10−C14 (and C19 in the case of **2**), but not the signals from the two symmetrically averaged trityl groups (C6−C9 and C15−C18). Compound **2** showed the pyridine signals of C19 and C10 at δ 152 and δ 138 ppm, respectively, which

(26) (a) Wamsler, T.; Nielsen, J. T.; Pedersen, E. J.; Schaumburg, K. *J. Magn. Reson.* **1981**, *43*, 387. (b) Tori, K.; Ogata, M.; Kano, H. *Chem. Pharm. Bull* **1963**, 235. (c) Montz, A. G.; Paul, D. B. *Aust. J. Chem.* **1969**, *22*, 1305. (d) Itai, T; Natsame, S. *Chem. Pharm. Bull.* **1963**, *11*, 83.

TABLE 2. Selected Signals in the ^{13}C NMR Spectra from Rotors 2, 3, and 3O in CDCl$_3$

Signal	2ᵃ δ	2-d_2ᵇ δ	3ᶜ δ	3-d_{30}ᵃ δ	3Oᶜ δ
1	126.5		128.9	128.6	136.2
2	141.9	141.9	146.1	145.8	144.0
3	84.3	84.5	82.2	81.8	80.2
4	100.7	100.7	102.1	101.8	109.4
5	56.2	56.2	56.6	56.1	56.5
10	138.4				118.5
11	119.4	119.4			
12	81.5	81.6			76.0
13	97.4	97.4			102.4
14	56.1	56.1			57.0
19	152.2	152.3			

ᵃData determined with NMR spectrometer operating at 125 MHz. ᵇData determined with NMR spectrometer operating at 75 MHz. ᶜData determined with NMR spectrometer operating at 100 MHz.

are relatively far from the signals corresponding to the aromatic trityl stator between δ 129 and δ 126 ppm. Reasonably separated from the signals of the trityl groups, the latter signals seemed potentially suitable for variable temperature analysis and dynamics characterization in the solid state by VT ^{13}C CPMAS NMR. In contrast, the signal corresponding to C1 at δ 128.9 ppm in compound **3** overlaps with the trityl stator signals between 127−130 ppm. Based on this overlap, one may expect that rate determinations by analysis of VT ^{13}C CPMAS NMR in the solid state should be extremely difficult. However, as previously described, this overlap could be eliminated in the spectrum of compound **3**-d_{30}. The latter showed only a strong signal at δ 128.6 ppm and three very small triplets with a coupling constant $^1J_{CD} = 24$ Hz corresponding to the deuterated carbons C7−C9.

X-ray Studies. Single crystals of the pyridine-containing structure **2** were grown by slow evaporation of a 4:1 mixture of

THF and hexanes. Two polymorphs were obtained from samples of the pyridazine rotor **3**. One was a solvated structure obtained by slow evaporation of a saturated solution of CHCl$_3$, and the second one was a solvent-free crystal obtained by slow evaporation from EtOAc. Crystals of the pyridazine N-oxide **3O** were obtained by slow evaporation from CHCl$_3$ but turned out to be relatively poor due to their tendency to suffer microcrystalline fracture during the mounting process such that the structural model could not be refined to the same level of agreement as the other ones. Repeated recrystallization attempts of **3O** did not yield suitable single crystals, mainly due to their relatively fast decomposition in solution. Crystallographic acquisition and refinement data[27] for all crystals are listed in the Supporting Information, and their ORTEP structures illustrated in Figure 2. Crystal data from molecular rotor **2** was obtained at 100 K to compare with the previously published crystal data for the fluorophenylene derivative **1b** and the cyanophenylene analogue **1d**.

A comparison of the space groups and unit cell parameters indicates analogies between the crystal structures of the nitrogen heterocycles **2**, **3**, and **3O** and those of the substituted polar phenylenes **1b** and **1d** (Supporting Information). It is not surprising that crystal isomorphism should occur for structures with similar sizes and geometries that are able to take advantage of analogous supramolecular interactions. For trityl-containing compounds, it is well known that complementary aromatic edge-to-face interactions

(27) X-ray diffraction studies were performed on an Enraf-Nonius FR590 diffractometer with a CCD area detector ($\lambda_{MoK\alpha}$ = 0.71073 Å, monochromator: graphite). Frames were collected at T = 100 K (compound **2**) and T = 293 K (compounds **3** and **3O**) via ω/φ-rotation. Structure solution was carried out with SHELXS-97 (ref 27a) and SIR2004 (ref 27b) programs. Refinement and data output were carried out with SHELXL-97 (ref 27a) program included in the software package WingGX-Version 1.80.05. (ref 27c) All non-hydrogen atoms were refined anisotropically. C−H hydrogen atoms were placed in geometrically calculated positions using a riding model. Figures and the hydrogen-bonding interactions in the crystal lattice were performed with MERCURY-Version 2.2 (ref 27d). (a) Sheldrick, G. M. *Acta Crystallogr.* **2008**, *A64*, 112. (b) Burla, M.C.; Caliandro, R.; Camalli, M.; Carrozzini, B.; Cascarano, G. L.; De Caro, L.; Giacovazzo, C.; Polidori, G.; Spagna, R. *J. Appl. Crystallogr.* **2005**, *38*, 381. (c) Farrugia, L. J. *J. Appl. Crystallogr.* **1999**, *32*, 837. (d) Macrae, C. F.; Edgington, P. R.; McCabe, P.; Pidcock, E.; Shields, G. P.; Taylor, R.; Towler, M.; van de Streek, J. *J. Appl. Crystallogr.* **2006**, *39*, 453.

(28) (a) Scudder, M.; Dance, I. *J. Chem. Soc., Dalton Trans.* **1998**, 329. (b) Scudder, M.; Dance, I. *Dalton* **2000**, 2909. (c) Dance, I.; Scudder, M. *New J. Chem.* **1998**, *22*, 481. (d) Lacour, J.; Bernardinelli, G.; Russell, V.; Dance, I. *CrystEngComm* **2002**, *4*, 165.
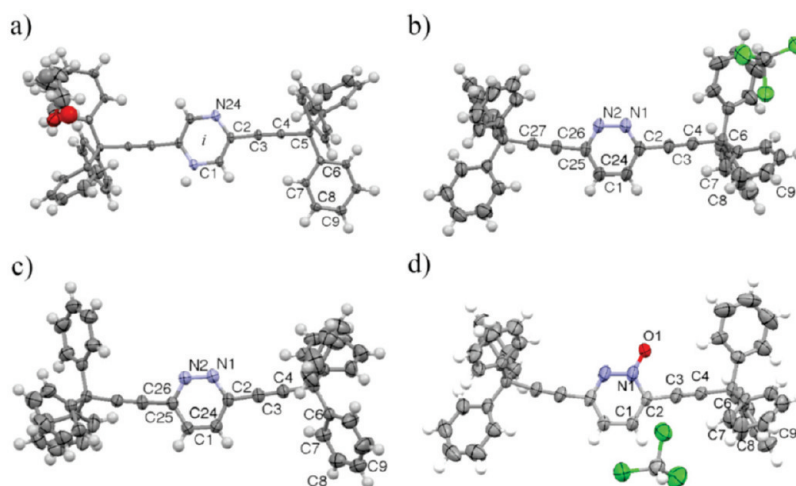
FIGURE 2. Molecular structures determined by single-crystal X-ray diffraction analysis of molecular compasses **2**, **3**, and **3O**: (a) average structure of compound **2** with positional disorder of the central pyridine; (b) structure of compound **3** in its CHCl₃ solvate; (c) solvent-free form; (d) structure of **3O** with one of the two orientations of the *N*-oxide rotator.
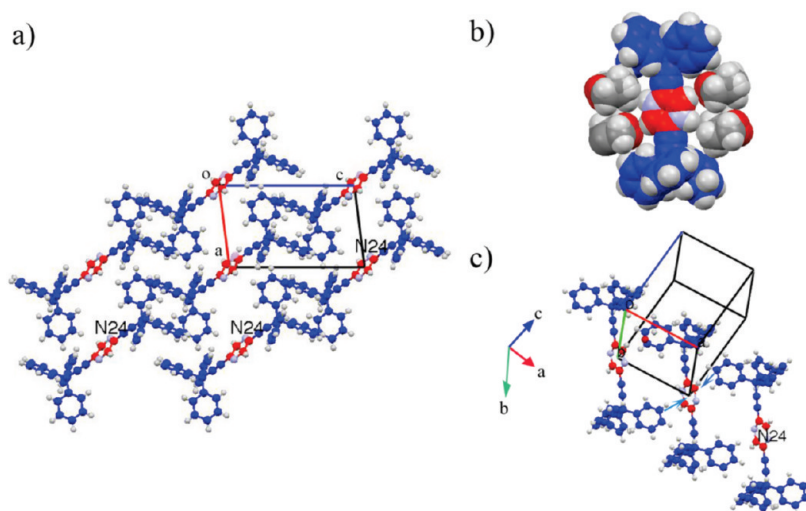

FIGURE 3. (a) Packing diagram of compound **2** (P-$\bar{1}$) down the *b*-axis acquired at 100 K with the THF molecules removed for clarity showing chains of rotors aligned by a 6-fold phenyl embrace (highlighted in the unit cell). (b) Space-filling diagram illustrating the four THF molecules arranged in antiparallel pairs that surround the diethynylpyridine fragment. (c) Additional edge-to-face interactions (shown in light blue) between the heteroaromatic rotator and two neighboring stator phenyl rings.

between adjacent Ph₃X groups (XPh₃----Ph₃X) are excellent directors of the crystal lattice in the form of a 6-fold phenyl embrace (6PE) involving adjacent groups.[28] As expected from the packing effects of the trityl groups, the N-hetero-aromatic structures showed similarities to the benzene-containing structures of **1a−f** in space group and unit cell parameters. The molecular and packing structures of the THF clathrate of pyridine rotor **2** are very similar to those of the benzene clathrate structures of **1a−f**. A comparison of crystals from compounds **2** and **1b** at 100 K shows that both occur in the space group P-$\bar{1}$ with very similar unit cell constants with the polar group positionally disordered with 50% occupancies in sites related by the crystallographic center of inversion. A simple replacement of the C−F for N fragments results in unit cell axes that vary between 0.6 and 4% and unit cell angles that fall within 0.8−3.5°.

The packing structure of compound **2**, like those of the benzene clathrates of **1a−e**, is characterized by having all

molecules in layers and aligned in the same direction in chains formed by trityl groups experiencing the 6-fold phenyl embrace 6PE (Figure 3a). The arrangement of THF molecules in **2** is also similar to that observed in all the benzene clathrates of **1a−d** with the solvent molecules arranged in antiparallel pairs with centroid-to-centroid distances of 2.59 Å and close to the diethynylpyridine moiety. One of the THF molecules on each side of the pyridine rotator directs its oxygen toward the C-1 carbon with a close contact of 2.46 Å, as expected for a C−H····O hydrogen bond (Figure 3b). The other THF molecules have a hydrogen-bonding interaction with the pyridine nitrogen, as suggested by a N$_{Pyr}$····H$_{THF}$ distance of 3.17 Å. One additional contact with a distance of 2.85 Å between the H12 atom from a neighbor stator and the pyridine ring centroid is observed in both faces of the pyridine rotator (Figure 3c).

The formation of monoclinic crystals for the pyridazine structures **3** is also reminiscent of the polar phenylenes as

exemplified by the structure of the cyano derivative **1d**. The three-dimensional array of oblique layers that constitutes the $P2_1/c$ crystal packing of compound **1d** is illustrated in the unit cell of Figure 4a. Each layer is based on adjacent pairs of rotors interacting though the edge-to-face 6-fold phenyl embrace (labeled 6PE in Figure 4a) and by close contacts with parallel displaced neighboring stators (blue arrows) showing opposite alignment of the dipoles between pairs of rotors. An additional close contact occurs between the cyano functional group and a neighboring stator phenyl group with a distance $CN\cdots H_{Ph}$ of 2.85 Å.

The crystal structure of the pyridazine rotor **3** was also solved in a monoclinic system with a space group $P2_1/n$ with molecules aligned along the $a-c$ diagonal. Despite differences in unit cell dimensions, the structure of **3** is closely related to that of **1d**. There is only a small difference in the volume of 1.6% ($\Delta V \sim 55$ Å^3) and nearly the same unit cell angles ($\Delta\beta = 0.85°$). An oblique array of layers similar to that present in **1d** formed by pairs of pyridazine rotors can be observed (Figure 4b). The structure also display lateral edge-to-face interactions between contiguous molecules (Figure 4b, blue arrows) with distances varying from 2.37 to 2.87 Å, which are shorter than those observed in **1d**.
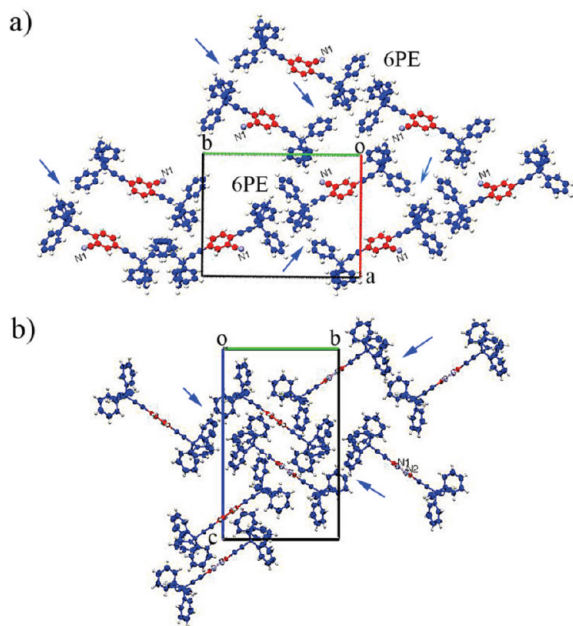

FIGURE 4. (a) View down c axis of the packing of **1d** showing the substituted phenylene in red (with the cyano group in light blue) and the trityl stators in blue. Six-fold phenyl embraces between adjacent trityl stators and additional edge-to-face interactions are indicated by 6PE and blue arrows respectively. (b) Packing of **3** with a view down a axis that highlights its analogy to that of **1d**, also showing interacting neighbors with lateral edge-to-face interactions pointed by blue arrows.

The crystal structure of **3O** could be best described by a model that includes an orientational disorder over two different positions of the crystal lattice where the oxygen atom of the N−O bond may occupy either of the two nitrogen atoms of the pyridazine ring. The two orientations of the N−O bond (A and B) are related by a 180° rotation about an axis perpendicular to the principal axis of the

molecule where the occupancy of the oxygen was freely refined and determined to be in a ratio of 70:30.

Tendencies for isomorphism within the heterocylic compounds are also evident by comparing the CHCl₃-containing structures with closely-related space groups $P2_1/c$ and $P2_1/n$. The crystallographic arrangement of pyridazine N-oxide **3O** and pyridazine rotor **3** shows structures with a periodic alignment along the c crystallographic axis and the $a-c$ diagonal, respectively, with interdigitated, antiparallel arrangement of rotors (not shown). Adjacent molecules of the pyridazine N-oxide present two types of intermolecular interactions (a) the disordered oxygen atom O1B acting as a donor toward the CHCl₃ with a $N2\cdots H_{solv}$ distance of 3.00 Å while the chlorine atom Cl1 interacts with a neighboring stator phenyl ring and (b) a pair of self-complementary weak interactions between oxygen O1A and the C−H group of one of the trityl phenyl rings which forms a 16-membered centrosymmetric ring. As shown in Figure 5a, this interaction involves atoms N1−O1A$\cdots$H14−C14 with a N1−C14 distance of 4.19 Å and a O1A$\cdots$H14−C14 angle of 135.42°. In a similar fashion, layers of pyridazine−solvate rotor **3** are based on dimeric motifs with nitrogen atoms acting as the donors toward the hydrogen of the solvent with $N2\cdots H47_{solv}$ distance of 2.65 Å and a $N2\cdots H47-C_{solv}$ angle of 141.37°, with the chlorine atom from the solvent acting as a donor toward a stator phenyl ring of its counterpart (Figure 5b).

Some of the main features in the X-ray-determined molecular structures of compounds **2**, **3** and **3O**, the parent hydrocarbon **1a**, and the fluorophenylene analogue **1b** are included in Table 3 with parameters defined with atom numbers shown in the structures in Scheme 5. Listed in the first three columns in Table 3 are the dihedral angles of the trityl phenyl groups, which define their helical chirality (M or P) and whether the molecular rotor is chiral (MM and PP) or meso (MP). The overall conformation of the molecules is such that the C−Ph bonds of the two trityl groups adopt an eclipsed relation and the fourth column contains the smallest dihedral angle between the plane of the central phenylene and one of such trityl C−Ph bond vectors. This position defines the minimum energy structure for the rotator in the frame of reference of the crystalline stator. The last three columns give a measure of the distortion experienced by each of the structures in terms of deviations from an idealized linear diyne axle. The fifth column lists the angle formed by a vector that extends between the two trityl carbons and one of the two alkyne carbons (C5A−C5−C3), and in the final column is the angle formed by vectors going from the trityl carbon to the centroid of the rotator to C1. While these values should be 0° and 60° for a perfectly linear structure, variations in Table 3 range from 1.5 to 12.3° and from 58.2 to 68.6°. With isomorphous crystal structures and only half a molecule per asymmetric unit, the molecular structures of compounds **1a**, **1b**, and **2** are relatively similar with distortions from linearity in the form of a letter "S", as expected from the crystallographic inversion center. The trityl phenyl rings (Ph1, Ph2, Ph3 in Table 3) in compound **2** adopt torsion angles ranging from 28° to 60° with propeller structures that, as required by crystal symmetry, adopt enantiomeric conformations with torsion angles of opposite sign.

Rotational Exchange Dynamics by Variable-Temperature ¹³C CPMAS NMR. High-resolution ¹³C NMR spectra can
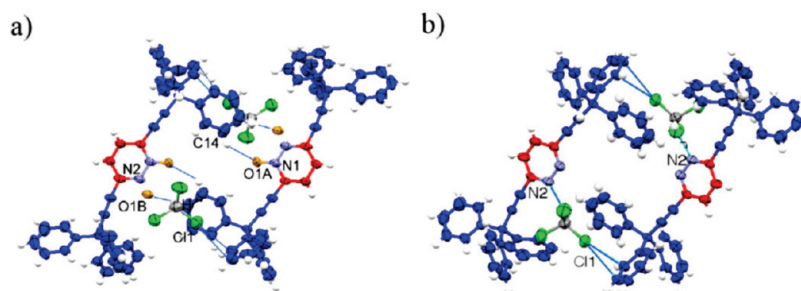
FIGURE 5. (a) Neighboring molecules of **3O** showing complementary N1A−O1A···H14−C14 contacts between the pyridazine ring (shown red) in one molecule and one of the trityl phenyls (in blue) and close contacts between the *N*-oxide with the smaller occupancy (N2−O1B), a chloroform molecule, and an adjacent ring: NO1B···HCCl$_3$ and Cl1···Ph. (b) Analogous arrangement in **3** with pyridazine, chloroform, and trityl phenyl involved in complementary N2···HCCl$_3$ and Cl1···Ph contacts.
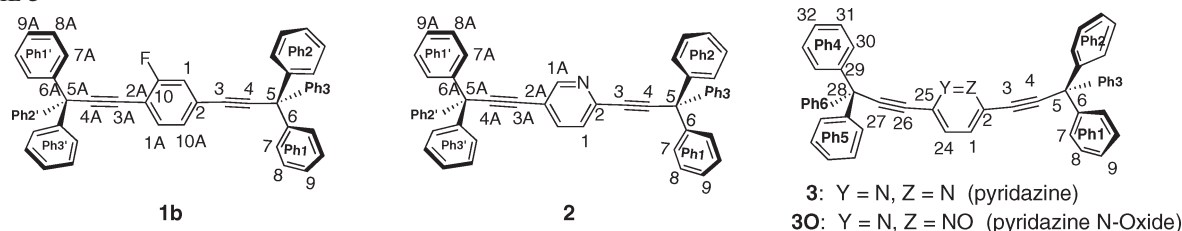
SCHEME 5

TABLE 3. Selected Distances, Angles, and Dihedral Angles from Crystal Data of Parent, Fluoro, Pyridine, Pyridazine, and Pyridazine *N*-Oxide Molecular Rotors

| molecular rotor | torsion angles C4−C5−C6-C7 (deg) | | | C1−C2−C5−C6 (deg) | d(C5−C5A)^a (Å) | C5A−C5−C3 (deg)^a | C5−centroid−C1 (deg) |
	Ph1	Ph2	Ph3				
1a^b (C$_6$H$_6$)	28.6	47.9	50.3	5.39	11.012	1.8	61.57
1b^c (C$_6$H$_6$)	27.0	50.2	50.4	1.0	11.032	1.5	58.20
2 (THF 100 K)	28.5	57.9	30.6	14.83	10.946	2.3	58.91
3^d (CHCl$_3$)	39.5	51.2	46.1	−5.98	10.833	8.7	66.52
	35.9$_{Ph4}$	9.4$_{Ph6}$	68.0$_{Ph5}$			7.2	
3^d	52.0	53.4	21.4	0.44	10.810	7.5	66.84
	−53.1$_{Ph4}$	−24.4$_{Ph6}$	−42.8$_{Ph5}$			9.4	
3O^d (CHCl$_3$)	40.7	46.2	49.2	1.09	10.801	12.3	68.59
	29.6$_{Ph4}$	16.8$_{Ph6}$	68.4$_{Ph5}$			9.0	

^{a}In compounds **3** and **3O** atom C5A corresponds to C28. ^{b}Reference 15. ^{c}Values obtained from the positional disorder at C1, when the fluorinated position is eclipsed with a phenyl ring (ref 9). ^{d}These structures have no internal symmetry.

be obtained in the solid state by taking advantage of rapid magic angle spinning and broadband ^{1}H decoupling. These are used to remove the strong heteronuclear dipolar interactions and chemical shift anisotropy that are responsible for the exceedingly broad spectra that is normally observed with solid samples.[29] With ^{13}C line widths on the order of 10−50 Hz obtained in this manner, it is often possible to distinguish signals of carbon atoms that are dynamically averaged in the solution but are crystallographically and magnetically nonequivalent in the solid state. In order to determine the rotational exchange dynamics of the nitrogen heterocycles in crystals of **2** and **3** one can take advantage of the fact that rotation of the aromatic groups about the dialkyne axle changes the position of the atoms on either side of the ring with respect to the frame of reference of the bis(trityl) stator, giving rise to signals that are crystallographically and magnetically nonequivalent. With reference to compound **2** (Figure 6), single-crystal X-ray diffraction at

100 K indicates that the pyridine nitrogen of any given molecule preferentially occupies one of the two positions related by rotation about the triple bonds. The X-ray structure shows that occupancy of one site (site "b" in Figure 6) is significantly greater than the occupancy on the other (site "a"), indicating an asymmetric rotational potential. Insufficient difference in electron density prevented the assignment of the occupancy factors in both sites.

The consequences of an asymmetric potential from a dynamic VT NMR perspective are that the line shapes of each of the exchanging signals should vary asymmetrically, as illustrated in Figure 6. Taking the carbon atom adjacent to the nitrogen as an example, one would expect two relatively sharp signals of different intensity for the sites Ca and Cb at relatively low temperatures, under conditions where the exchange frequency is much slower than the frequency difference between the two peaks (slow exchange regime). The relative intensity of the two peaks would be directly proportional to the temperature-dependent population of the rotator in the two sites, potentially providing a direct measure of their free energy difference. An increase in the

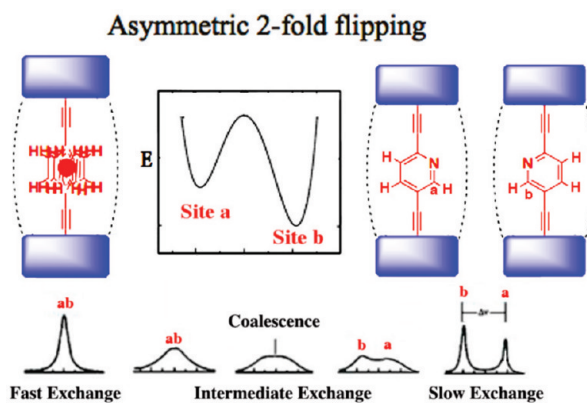(29) Fyfe, C. A. *Solid State NMR for Chemists*; CFC Press: Guelph, Ontario, 1984.

Asymmetric 2-fold flipping

FIGURE 6. Illustration of the changes in line shape in a high-resolution NMR spectrum of a given rotator nucleus that can occupy two distinct sites in an asymmetric 2-fold flipping potential in the fast, intermediate, and slow exchange regimes. The same qualitative behavior is expected for all magnetically distinct nuclei that exchange between sites a and b, including the ^{13}C NMR signals acquired by high-resolution CPMAS spectra.

exchange rate as the temperature increases would cause the two peaks to broaden until they collapse into a single broad signal at the coalescence temperature. Further heating and faster exchange rates are expected to sharpen the resulting line into a single one with a chemical shift that is the population-weighted average of the two original frequencies for sites a and b.

VT ^{13}C CPMAS NMR of Pyridine Molecular Compass 2. Polycrystalline samples of the THF solvate of the molecular compass **2** were analyzed by ^{13}C CPMAS NMR to determine whether it would be possible to resolve rotator signal corresponding to the nonequivalent sites of the pyridine rotator related by a 180° site exchange. Variable-temperature solid-state NMR experiments were performed from 165 to 386 K while the presence of THF in the samples was monitored. A spectrum acquired at 298 K showed THF carbon signals at 67 and 36 ppm, and by analogy with the solution spectrum, the relatively broad signals around 152 and 138 ppm were attributed to C19 and C10 from the central pyridine (Figure 3b). Support for these assignments was obtained by acquiring a spectrum with a dipolar dephasing pulse sequence (also known as nonquaternary carbon suppression or NQS pulse sequence),[30] which is used to remove the strongly coupled C−H signals. The NQS spectrum contained signals of the aromatic trityl *ipso*-carbons at δ 144, 142, and 141 ppm, the four alkyne carbons at 101, 96, 84, and 81 ppm, and the two isochronous trityl methane carbons at δ 54 ppm. Also seen in the NQS spectrum were the signals of the relatively mobile THF molecules at 67 and 36 ppm, as expected for hydrogenated carbon atoms with weak dipolar coupling due to the rapid motion of the THF carbons.

Assuming that the broad nature of the pyridine signals was an indication of a dynamic 2-fold rotary process in the intermediate exchange regime we measured the spectrum at 165 K, the lowest attainable temperature for our CPMAS probe. To our disappointment, we did not observe a splitting

(30) Alemany, L. B.; Grant, D. M.; Alger, T. D.; Pugmire, R. J. *J. Am. Chem. Soc.* **1983**, *105*, 6697. The NQS experiment was accomplished by turning the hydrogen broadband decoupler off for 50 μs after cross polarization and before signal acquisition.

of the signals of C19 and C10, which remained relatively broad (Figure 7a). Following this, we increased the temperature of the sample to 386 K, and we saw the signals of THF disappear and the signals of C19 and C10 to become sharp (Figure 7a), as expected for a fast exchange process. While cooling the sample again increased the line width of C19 and C10 to the levels observed before the loss of solvent, we were not able observe their splitting into signals that could be assigned to the different slowly exchanging sites. As indicated below, information on the dynamics of **2** was available by taking advantage of ^{2}H NMR.

VT ^{13}C CPMAS NMR of Pyridazine Molecular Compass 3-d_{30}. As expected from the small chemical shifts dispersion observed in the ^{13}C NMR solution spectrum, the aromatic region of the ^{13}C CPMAS NMR of natural abundance **3** consisted of two sets of overlapping signals in the ranges of 148−143 and 135−125 ppm (Figure 8a). Knowing that the signals of the pyridazine carbons (C1 and C24, from the crystal structure) completely overlap with all the aromatic CH signals of the two trityl groups, and as previously
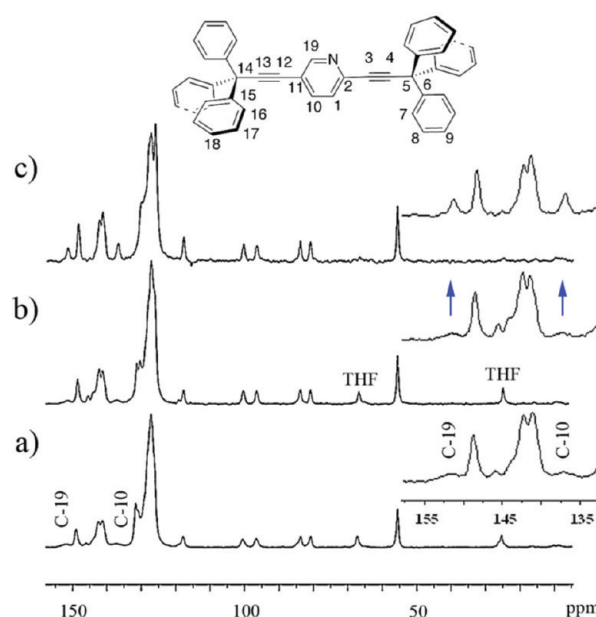

FIGURE 7. Solid-state ^{13}C CPMAS NMR spectra of compound **2** at (a) 165 K with broadened signals for C19 and C10, (b) 296 K, and (c) 386 K with sharpened C19 and C10 signals and the loss of THF.

demonstrated with samples **1a**-d_{30}, we decided to explore the use of perdeuterated trityl groups with the purpose of selectively highlighting the signals of C1 and C24 in **3**-d_{30} by cross-polarization from their attached hydrogen atoms. With an optimized cross-polarization contact time to only transfer magnetization from H1 and H24 to their closest carbon signals (C1, C2, and C3) we were able to obtain spectra where only the pyridazine carbons can be observed (Figure 8). The signals corresponding to the hydrogenated carbons C1 and C24 appeared at 296 K as a broad signal centered at δ 130 ppm (labeled C1 in Figure 8c). Unfortunately, as illustrated by parts b−d of Figure 8, variations in temperature over a range of more than 200 K (167−385 K) showed no variations in line shape, suggesting that there is no significant differences in the shielding values for the two

orientations of the pyridazine ring or that there is no motion in this temperature range due to a very high energy barrier. One may speculate on whether the large deviation from the linearity observed in the crystal structure may be responsible for a large rotational barrier.
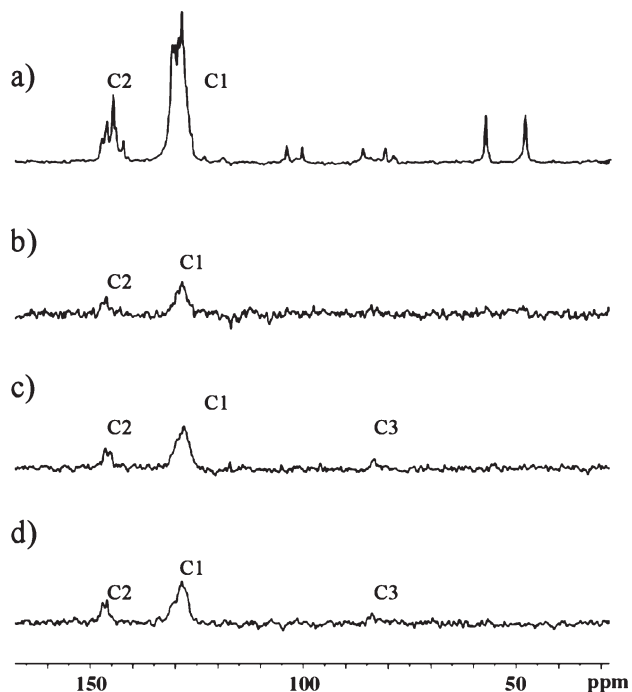

FIGURE 8. ^{13}C CPMAS NMR of microcrystalline samples of compound **3** with natural abundance carbons (a) and with isotopolog **3**-d_{30} at (b) 385, (c) 296, and (d) 167 K. No changes were observed to the signals corresponding to C1.

CPMAS NMR of Pyridazine *N*-Oxide Molecular Compass 3O. Solid-state NMR experiments at room temperature were carried out with samples of compound **3O** prepared from a saturated solution in chloroform. Unfortunately, very broad lines in the aromatic region of solid-state NMR suggested a great deal of disorder. All attempts to obtain sufficiently large samples of crystalline material were hampered by sample decomposition so that no further tests were pursued on this molecular rotor.

Solid-State NMR Dynamics: Variable-Temperature Line-Shape Analysis of ^{2}H NMR. Quadrupolar echo ^{2}H NMR spectroscopy is a powerful tool that can be used to determine internal molecular dynamics of molecular rotors.[31–33] The method is based on the fact that changes observed in the spectrum of powder samples as a function of temperature can be analyzed in terms of dynamic process that change the orientation of the C−D bond vector with respect to the orientation of the external magnetic field. In fact, ^{2}H NMR spectroscopy is largely dominated by the orientation-dependent interaction between the nuclear spin and electric quadrupole moment at the nucleus. Thus, a single crystal with only one type of C−^{2}H bond with a symmetric quadrupolar tensor would give a doublet with a quadrupolar splitting $\Delta\nu$ that depends on the orientation angle β that the bond

makes with respect to the external field.[34]

$$\Delta\nu = \frac{3}{4}(e^2 q_{zz}Q/h)(3\cos^2\beta - 1) = \frac{3}{4}\text{QCC}(3\cos^2\beta - 1)$$

where Q represents the electric quadrupole moment of the deuterium, e and h are the electric charge and Planck constant, and q_{zz} is the magnitude of the principal component of electric field gradient tensor, which lies along the C−^{2}H bond. The frequency difference for signals of pyridine C−^{2}H bonds, which have a QCC = 178 kHz,[35] changes from 267 kHz when $\beta = 0°$ and 133.5 kHz for $\beta = 90°$, to 0 kHz when the C−^{2}H bond is oriented at the magic angle of $\beta = 54.7°$. A collection of doublets in all possible orientations in a powder sample gives rise to a broad symmetric spectrum with two maxima and two shoulders known as a Pake or powder pattern. Variations in the powder pattern of a solid sample occur when the C−^{2}H bonds experience reorientations between different sites with exchange rates in a range of ca. $10^3–10^8$ s^{-1}.[36] Line-shape analysis of the deuterium NMR spectra allows for a characterization of the frequency and type of motion in terms of discrete jumps between different sites or continuous rotation.

For our studies on molecular compasses and gyroscopes, we take advantage of the well-characterized spectral changes that occur upon rotation of an aromatic group about its 1,4-axis.[37–39] In the case of compound **2**-d_2, measurements were carried out between 250 and 340 K at 46.07 MHz with a quadrupolar echo sequence that uses a 90° pulse of 2.25 μs followed by dephasing and refocusing delays of 42 and 50 μs, respectively, and the relaxation time between pulses was 20 s. As the ^{2}H label only represents 0.3% of the total mass in the sample, at least ca. 3500 transients had to be averaged to obtain reasonable spectra. As a point of reference, ca. 10000 transients were obtained at room temperature. In the left column of Figure 9 we illustrate the results of measurements carried out at 270, 296, 310, and 322 K processed with a line broadening function of 4.5 kHz.

As illustrated in Figure 9, variations in the spectrum with increasing temperature were most noticeable in the relative intensity of the peaks at $\Delta\nu = \pm 64$ kHz, which evolved from two relatively narrow maxima at 270 K to two broad shoulders as temperature increased towards the fast exchange limit. These changes are accompanied by a substantial intensity increase of the peaks at the center of the spectrum at $\Delta\nu = \pm 17$ kHz. The line shape simulations,[40] shown to the right of the experimental spectra in Figure 9, were carried out with a model where the geometry of motion is limited to discrete jumps related by an angular displacement

(31) Sillescu, H. *Pure Appl. Chem.* **1982**, *54*, 619.

(32) Spiess, H. W. *Colloid Polym. Sci.* **1983**, *261*, 193.

(33) Hoatson, G. L.; Vold, R. L. *NMR Basic Princ. Prog.* **1994**, *32*, 1.
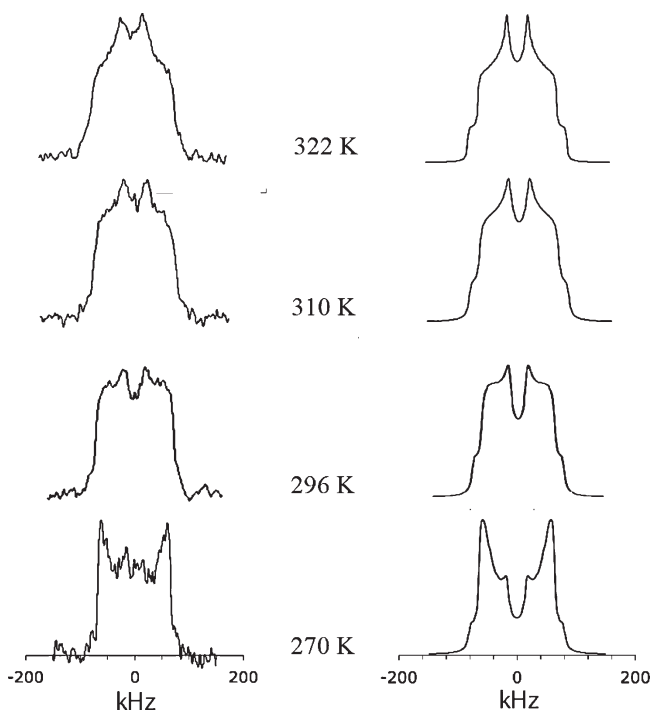
(34) This equation assumes negligible asymmetry in the electric field gradient tensor: $\eta = (q_{xx} - q_{yy})/q_{zz} = 0$. Deviations from this condition are generally small for aromatic deuterons.

(35) Barnes, R. G.; Bloom, J. W. *J. Chem. Phys.* **1972**, *57*, 3082.

(36) Duer, M. *Introduction to the Solid State NMR Spectroscopy*; Blackwell: Oxford, UK, 2004.

(37) Cholli, A. L.; Dumais, J. J.; Engel, A. K.; Jelinski, L. W. *Macromolecules* **1984**, *17*, 2399.

(38) Rice, D. M.; Witebort, R. J.; Griffin, R. G.; Meirovich, E.; Stimson, E. R.; Meinwald, Y. C.; Freed, J. H.; Scheraga, H. A. *J. Am. Chem. Soc.* **1981**, 103.

(39) Rice, D. M.; Meinwald, Y. C.; Scheraga, H. A.; Griffin, R. G. *J. Am. Chem. Soc.* **1987**, *109*, 1636.

(40) Nishikiori, S. I.; Soma, T.; Iwamoto, T. *J. Inclusion Phenom. Mol. Recognit. Chem.* **1997**, *27*, 233.

(41) Macho, V; Brombacher, L; Spiess, H. W *Appl. Magn. Reson.* **2001**, *20*, 405.

FIGURE 9. Experimental (left) and simulated (right) solid-state ^{2}H NMR of samples of **2**-d_2. The rotation rate constants for 2-fold exchange from bottom to top are (10^6 s^{-1}): 0.50, 4.0, 8.0, and 14.

of 180° with a quadrupolar coupling constant of QCC = 180 kHz for the two aromatic deuterium.[41] The model assumes that the angle made by the C—D bond vector with respect to the axis of rotation is 60°, even though small deviations (±2.4°) are observed in the crystal structure. While variations in the population of the two sites of simulated spectra significantly affect the distance between two central lines in the spectrum, the best simulations suggest a ratio of ca. 55:45 for the two sites with no improvements observed when the site population was changed as a function of temperature. As shown in Figure 9, spectral variations between 270 and 322 K were reasonably well simulated with exchange rates varying from 0.5×10^6 to 14×10^6 s^{-1}. Assuming that the rotary site exchange values (k_{ROT}, in Hz) represent a first-order process well described by the Arrhenius equation, $\ln k_{ROT} = \ln A - (E_a/R)(1/T)$, we determined the activation energy (E_a) and pre-exponential factor (A) for the 2-fold site exchange in the case of **2**-d_2 as 8.5 kcal/mol (35.56 kJ mol^{-1}) and 6.2×10^{12} s^{-1}, respectively. A comparison of the activation energy of the pyridine rotator in **2**-d_2 with those previously reported for phenylene (**1a**-d_4), fluorophenylene (**1b**-d_3), and difluorophenylene (**1f**-d_2) rotators indicates substantially less hindering for the nitrogen heterocycle. Activation energy values for **2**-d_2, **1a**-d_4, **1b**-d_3, and **1f**-d_2 are 8.5 (35.56 kJ mol^{-1}), 12.8 (53.55 kJ mol^{-1}), 13.7 (57.32 kJ mol^{-1}), and 14.8 kcal/mol (61.92 kJ mol^{-1}), respectively. It is reasonable that the larger fluorine substituent should increase the activation energy value, and one may attribute the lower E_a value in **2**-d_2 to the smaller steric hindrance of the pyridine moiety and the smaller size of the included THF.

Conclusions. The expectations based on the smaller size of the pyridine rotator were met by the experimental results. It is interesting that substitution of one carbon atom by one nitrogen has no negative effect in the crystalline arrangement, which seems to be determined by the size and shape of the two trityl groups and the complementary edge-to-face interactions of their 6-fold phenyl embrace. With the results from this study we have shown a suitable synthetic procedure for the synthesis of molecular compasses with heterocyclic rotator while improving our understanding of rotary dynamic in the solid state. Future studies will address a combination of polar rotators and bulkier stators in search of lower rotational barriers in materials where thermal excitations may be transported by dipole–dipole interactions in the form of optical phonons.

Experimental Section

General Method for the Synthesis of Heterocyclic Rotors. In a flame-dried round-bottom flask fitted with a condenser, 0.5 equiv of the corresponding heterocyclic compound (**5**, **5**-d_2, or **6**) was mixed with at least 1.1 equiv of 3,3,3-triphenylpropyne (**4** or **4**-d_{15}) under nitrogen atmosphere, and then diisopropylamine as base and THF as solvent were added in a 1:1 (v/v) relationship. The mixture was bubbled with nitrogen (20 min), and dichlorobis(triphenylphosphine)palladium(II) (0.05 equiv) and copper(I) iodide (0.1 equiv) were added afterwards. The mixture was refluxed overnight and cooled to room temperature, the reaction was quenched with saturated solution of ammonium chloride, and the organic layer was extracted with methylene chloride. The aqueous layer was extracted with methylene chloride three times. The combined organic layers were dried over Na$_2$SO$_4$, and the solvent was removed under high-pressure vacuum. The residues were purified by flash chromatography on silica gel or neutral alumina with a mixture of hexanes–CH$_2$Cl$_2$–ethyl acetate or hexanes–ethyl acetate as eluent.

The synthesis of compound **2** was performed following the above methodology. The crude of the reaction showed a yield of the desirable product above 80% by ^{1}H NMR. The compound was eluted on silica gel using hexane–DCM–EtOAc (96:2:2) to give the desired product in low yields (52 mg, 22 %): mp 282–284 °C; IR ν_{max} (neat) 3059, 3027, 2228, 1951, 1809, 1595, 1581, 1539, 1489, 1467, 1445, 1362, 1270, 1180, 1079, 1064, 1030, 1002, 848, 773, 752, 720, 660 cm^{-1}; HRMS calcd for C$_{47}$H$_{33}$N + H$^+$ 612.2685, found 612.2690; ^{1}H NMR (500 MHz, CDCl$_3$) δ 8.73 (1H, d, J = 2.0 Hz), 7.77 (1H, dd, J = 2.0, 8.2 Hz), 7.47 (1H, d, J = 8.2 Hz), 7.40–7.26 (30 H, m); ^{13}C NMR (125 MHz, CDCl$_3$) δ 152.1, 144.6, 144.5, 141.9, 138.4, 129.1, 129.0, 128.1, 128.0, 126.9, 126.8, 126.4, 119.4, 100.7, 97.4, 84.4, 81.5, 56.1, 56.0.

Characterization data for the remaining rotors are provided in the Supporting Information.

Supporting Information Available: Spectroscopic data ^{1}H and ^{13}C NMR and HRMS of compounds **2**, **2**-d_2, **3**, **3**-d_{30}, **3O**, **5**-d_2, and **6**; X-ray diffraction data for compounds **2**, **3**, and **3O** (table of parameters and CIFs). This material is available free of charge via the Internet at http://pubs.acs.org.